Novel Fe^{2+} oxidation states in infinite-layer Sr_2FeIrO_4

1 Computational Details

Theoretical calculations are performed based on first-principles density functional theory (DFT) method with the PBE generalized gradient approximation (GGA) implemented in Vienna *ab initio* Simulation Package (VASP). The strong-correlated correction is considered with GGA+U method. The effective onsite Coulomb interaction parameter U_{eff} is set to be 4 for Fe and 2.5 for Ir.

A $11 \times 11 \times 11$ k-point grid is used for geometry optimization with fixed volume, while a $15 \times 15 \times 15$ grid is generally used for calculating Density of States and partial charge density. A $2 \times 2 \times 2$ supercell is used for calculating magnetic coupling constants. Maximum allowed error in energy is set to 10^{-4} eV.

All U values were extracted from Ref. [1]. Test runs were carried out on Sr_2CeIrO_6 (<0.01Å error) and Sr_2FeRuO_6 (0.05Å/7.87Å error).

2 Results and Discussion

2.1 Geometry

Lattice parameters is highly affected by stoichiometry. Sr_2FeIrO_4 and $Sr_2FeIrO_{4.5}$ are the best matches (Figure 1).

We are unable to reproduce the short Fe-O bond length. Geometry optimisation is carried out for a completely non-symmetric starting guess with 1.64Å Fe-O distance and 2.36Å Ir-O distance. The optimised structure is fully symmetric, with equal Fe-O and Ir-O distance of 1.99Å, matching the 1.99554Å for $SrFeO_2$ in Ref. [2].

No geometric distortion of Oxygen polyhedra is predicted for Sr_2FeIrO_4.

2.2 Electronic configuration

Orbital energies of Sr_2FeIrO_4 are extracted from DOS (Figure 2), and occupancies are determined according to lm-projected DOS and its integration up to E_F (Table 1). A non-spin-polarized calculation has been carried out for comparison. $d_{x^2-y^2}$ orbitals directly overlap with O's.

The valence states of Sr_2FeIrO_4 is $Sr_2^{2+}Fe^{2+}Ir^{2+}O_4^{2-}$.

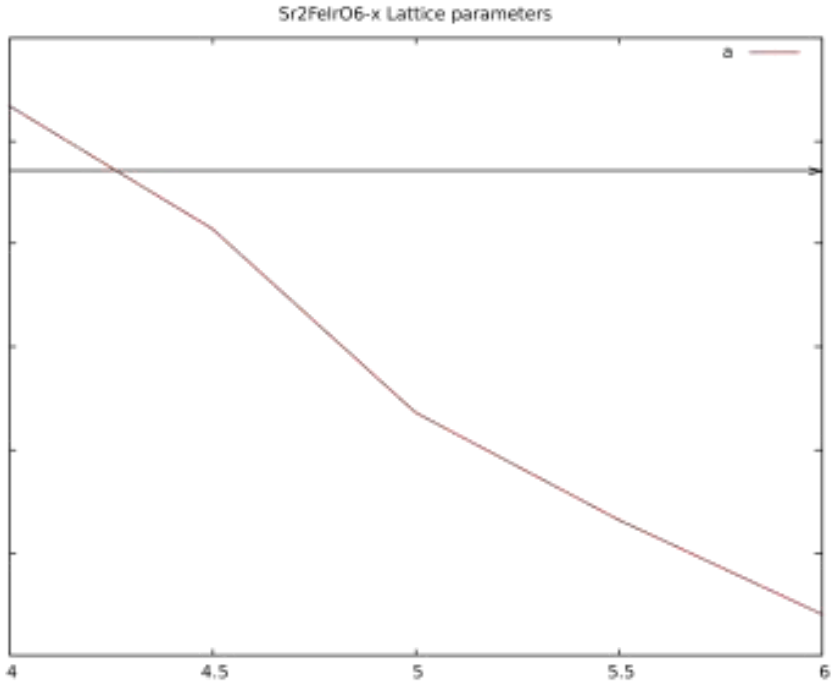

Figure 1: Lattice a

$Fe_{\uparrow}$	s 0.18 p_y 0.09 p_z 0.04 p_x 0.09 $d_{x^2-y^2}$ 1.03 d_{yz} 0.97 d_{z^2} 0.93 d_{xz} 0.96 d_{xy} 0.98
$Fe_{\downarrow}$	s 0.17 p_y 0.08 p_z 0.03 p_x 0.09 $d_{x^2-y^2}$ 0.18 d_{yz} 0.07 d_{z^2} 0.84 d_{xz} 0.07 d_{xy} 0.06
$O_{\uparrow}$	s 0.78 p_y 0.59 p_z 0.61 p_x 0.58 $d_{x^2-y^2}$ 0.00 d_{yz} 0.00 d_{z^2} 0.00 d_{xz} 0.00 d_{xy} 0.00
$O_{\downarrow}$	s 0.77 p_y 0.55 p_z 0.58 p_x 0.54 $d_{x^2-y^2}$ 0.00 d_{yz} 0.00 d_{z^2} 0.00 d_{xz} 0.00 d_{xy} 0.00
$Sr_{\uparrow}$	s 1.00 p_y 0.97 p_z 0.97 p_x 0.97 $d_{x^2-y^2}$ 0.02 d_{yz} 0.03 d_{z^2} 0.01 d_{xz} 0.03 d_{xy} 0.02
$Sr_{\downarrow}$	s 1.00 p_y 0.97 p_z 0.97 p_x 0.97 $d_{x^2-y^2}$ 0.03 d_{yz} 0.03 d_{z^2} 0.01 d_{xz} 0.03 d_{xy} 0.02
$Ir_{\uparrow}$	s 0.32 p_y 0.14 p_z 0.03 p_x 0.12 $d_{x^2-y^2}$ 0.47 d_{yz} 0.92 d_{z^2} 0.74 d_{xz} 0.90 d_{xy} 0.96
$Ir_{\downarrow}$	s 0.30 p_y 0.12 p_z 0.04 p_x 0.12 $d_{x^2-y^2}$ 0.42 d_{yz} 0.90 d_{z^2} 0.70 d_{xz} 0.88 d_{xy} 0.24

Table 1: Integrated PDOS – partial orbital occupancy

2.2.1 Fe

In the ferromagnetic case, he electronic configuration of Fe is $d^2_{z^2}d^1_{xy}d^1_{yz}d^1_{xz}d^1_{x^2-y^2}$(Figure 3).

While d_{z^2} is the highest-lying one among spin-up orbitals, it is doubly occupied. Similar behavior has been observed in SrFeO2. According to Pruneda *et al.*, a hybridization between $3d_{z^2}\uparrow$ and 4s orbital changes the shape of $3d_{z^2}\uparrow$ orbital and lowers the penalty when d_{z^2} gets doubly occupied. A strong hybridization between $3d_{z^2}\uparrow$ but not $3d_{z^2}\downarrow$ with 4s in DOS (Figure 4) and the eigenstate wave function of up- and down-spin d_{z^2} obtained by integrating charge density around the DOS peak over the entire Brillouin

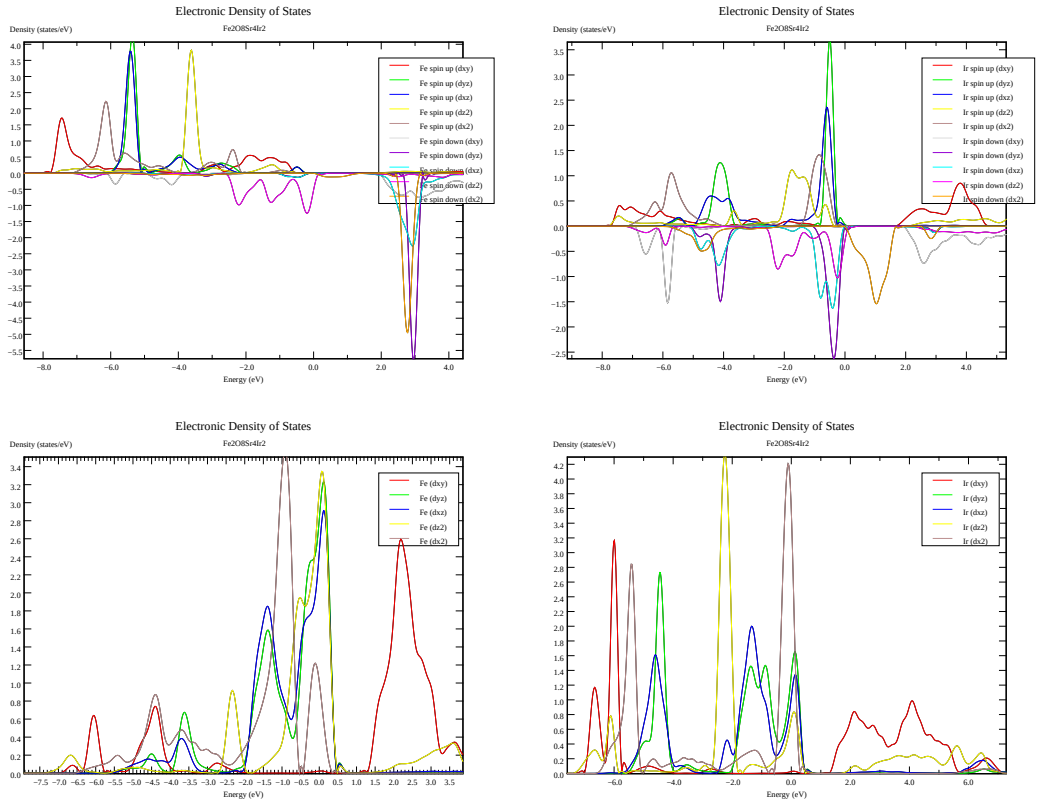

Figure 2: lm-projected DOS of Fe/Ir with/without spin polarization

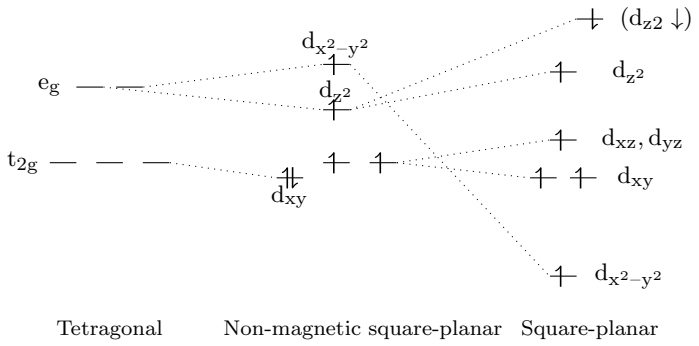

Figure 3: Fe orbitals

zone (Figure 5) both indicates the presence of such a mechanism in Sr_2FeIrO_4.

Magnetic interaction may also be responsible, although comparing magnetic and non-magnetic cases may not be reasonable. Non-spin-polarized calculation gives an orbital configuration of $d^2_{xy}d^1_{yz}d^1_{xz}d^1_{z^2}d^1_{x^2-y^2}$ instead of $d^2_{z^2}d^1_{xy}d^1_{yz}d^1_{xz}d^1_{x^2-y^2}$. Similarly,

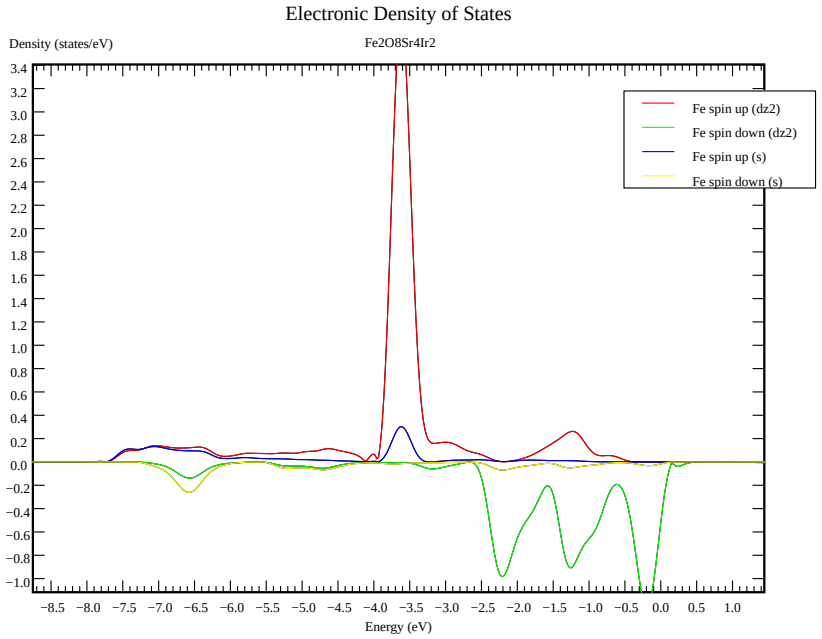

Figure 4: Hybridization between $3d_{z^2} \uparrow$ and $3d_{z^2} \downarrow$ and 4s orbitals

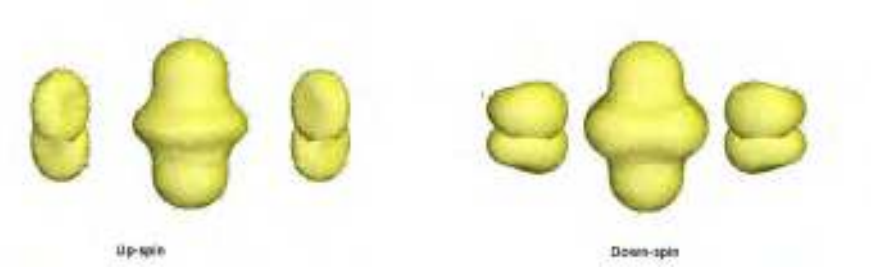

Figure 5: Eigenstate corresponding to $3d_{z^2} \uparrow$ and $3d_{z^2} \downarrow$ orbitals

the occupation of d_{z^2} orbital drops by 0.5e if all neigbours of the magnetic Fe is fixed to be diamagnetic, or if all neighbor atoms are of the opposite spin direction. In both cases, the electrons lost to d_{z^2} are scattered among the other orbitals, and the majority spin orbitals hybridize with the 4s orbitals a bit more significantly than the minority spin orbital (the difference is tiny and I am not certain). It seems, therefore, that the magnetic interaction also plays a part in shaping the orbital occupation. As the d_{z^2} orbital is less affected by magnetic coupling than most other orbitals, the penalty of down-spin electrons occupying the orbital is also less. The double occupation of d_{z^2} orbital, therefore, could be explained by magnetic interaction. Following similar lines of thought, the changes in orbital alignment from the non-spin-polarized case to the spin-polarize case can be better explained. $d_{x^2-y^2}$ becomes more energetically favorable due

to strong in-plane ferromagnetic interaction, and so does d_{xy}, though to a less extent. However, as introducing diamagnetic ions may have significant impacts upon electronic structures, the analysis may be unreliable.

2.2.2 Ir

The intensity of Ir-O bonding-antibonding splitting predominantly shapes the Ir DOS (Figure 6, possibly due to the large radius of Ir. A significant gap (2eV) isolates all bonding and all antibonding d-orbitals (Figure 8). $d_{x^2-y^2}$ and d_{z^2} has the largest bonding-antibonding splitting, making the orbital occupation almost $0.5 \uparrow +0.5 \downarrow$. The d_{xy} orbital, for obvious reasons, is less affected by the splitting, allowing the magnetic interaction to spin-polarize this orbital completely. Even less splitting is present in the other two t_{2g} orbitals, and they are doubly occupied. To sum up, Ir is in low-spin configuration (in accordance with experimental data), but the responsible Ir-O bonding has significant covalent characteristics, unlike in the case of $e_g - t_{2g}$ splitting.

According to the speculative explanation above, Figure 7 shows the conceptual orbital diagram for Ir spin-up component. Its spin-down counterpart is almost the same except for the d_{xy} orbital propelled above the Fermi level by magnetic interactions. Besides, the splitting is also observed for calculations without GGA+U (Figure 9), which rules out the possibility that the gap is of Hubbard nature. Lastly, the d_{z^2} orbital exhibits multiple peaks (Figure 10), which hybridizes with Fe DOS, and the higher peaks have been assumed antibonding ones.

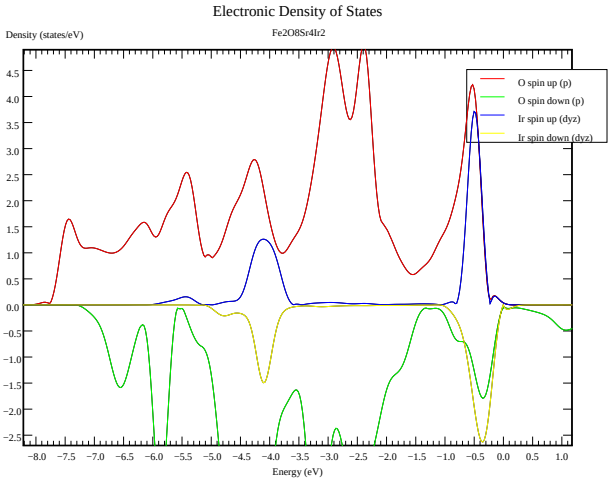

Figure 6: σ-bonding and antibonding between Ir and O

2.3 Charge transfer

All calculations are done with a supercell the size of two 'unit' cells. Each time, one O atom is inserted between an Fe and an Ir atom, increasing the O number from 8/two unit

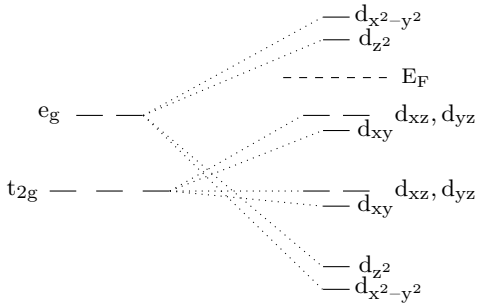

Figure 7: Ir↓ orbitals

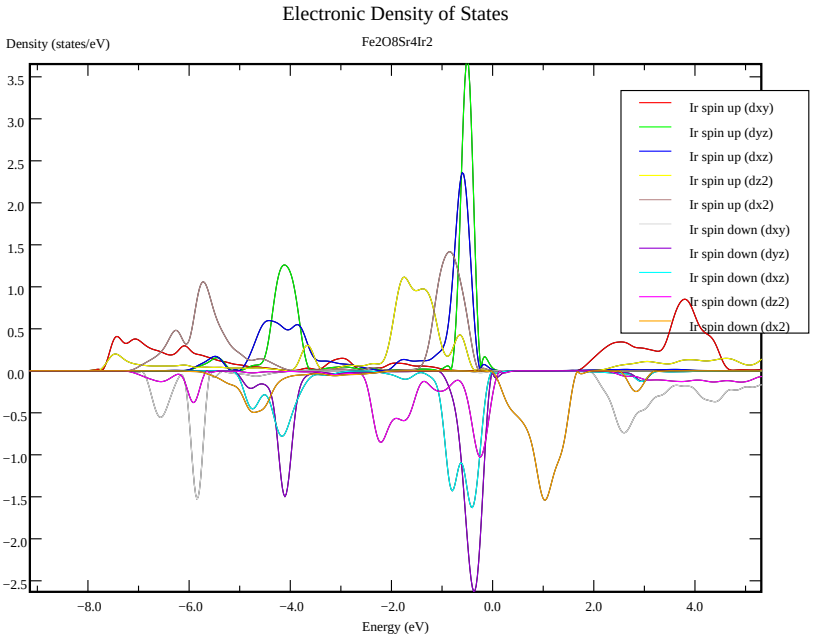

Figure 8: lm-projected DOS of Ir

cell to 12/two unit cell. The two Fe and Ir atoms with new neighbours each receive 0.5 electron every time (see Figure 11). The two Fe atoms, when their turn comes, promptly loses half an electron from $d_{z^2} \downarrow$ orbital to the newly-formed Fe-O bond[1], achieved a happier Fe^{3+} state with higher (approximately 4) magnetic moments (see Figure 12), and sticked to the configuration later on (see Figure 13). Apart from this, the RWIGS charges and the lm-decomposed charges of Fe exhibit no significant change, indicating that the lost electrons are of a non-localized nature. In summary, Fe atoms stick to

[1]Here an electron is presumed to be in a bond, when it cannot be seen in the projected DOS but is visible in Bader charge.

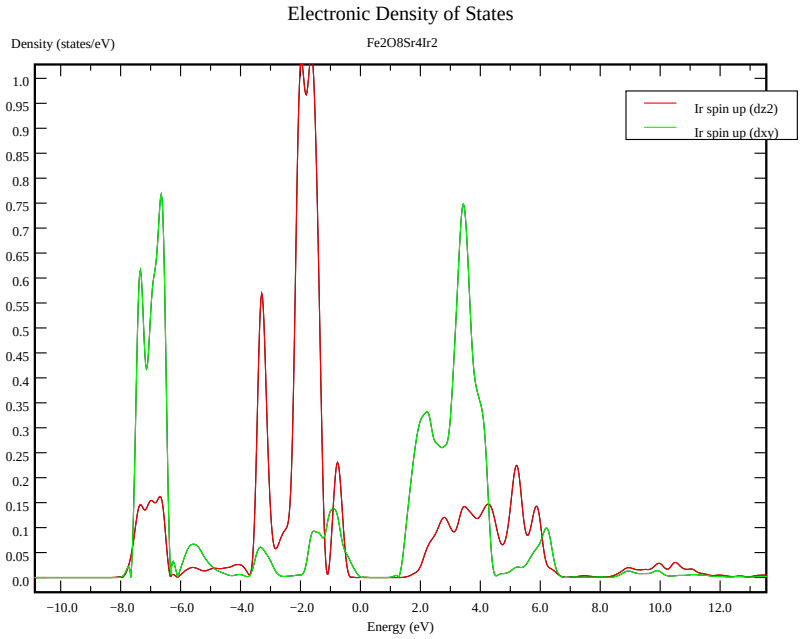

Figure 9: Splitting without Hubbard U

the comfortable configurations (Fe^{2+}, Fe^{3+}), and throw the extraneous electrons to the bonds.

As of Ir, changes in bonding/antibonding intensity are sufficient to explain the charge transfer involved. As the system is oxidized, occupation of all d up orbitals remain steady while the occupation of d-down orbitals gradually increase or decrease to a half-filled (0.5e) value, possibly due to stronger bonding-antibonding splitting (see Figure 14) caused by more oxygen and more slender cells.

2.4 Magnetic Coupling

The interplanar magnetic coupling is weakly antiferromagnetic ($E_{FM} - E_{AFM}$ ~4meV), in accordance with the experimental data.

3 Summary

No short Fe-O bond or distortion is predicted for Sr_2FeIrO_4. The d_{z^2} orbital of Fe is doubly occupied, possibly due to the combined effects of $3d_{z^2\uparrow}$-4s hybridization and in-plane magnetic interaction. The Ir-O bonds are of strong covalent nature, and the occupation of Ir orbitals is significantly affected by the bonding-antibonding gap. The model of charge transfer for Sr_2FeIrO_{6-x} is similar to that of La_2MnRhO_{6-x}, where ions retain the happier configuration (both Fe^{2+} and Fe^{3+} in this case) inside Wigner-Seitz

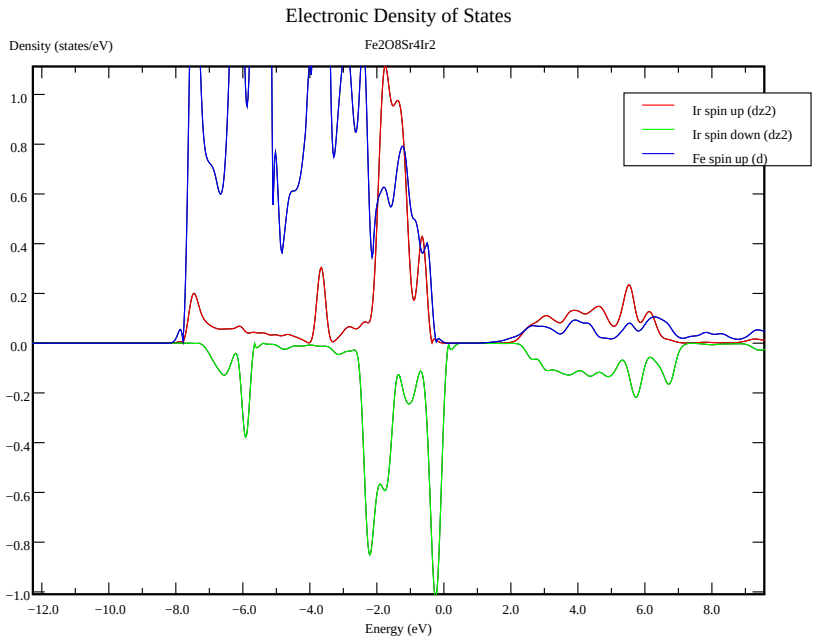

Figure 10: Multiple-peak pattern of Ir d_{z^2}

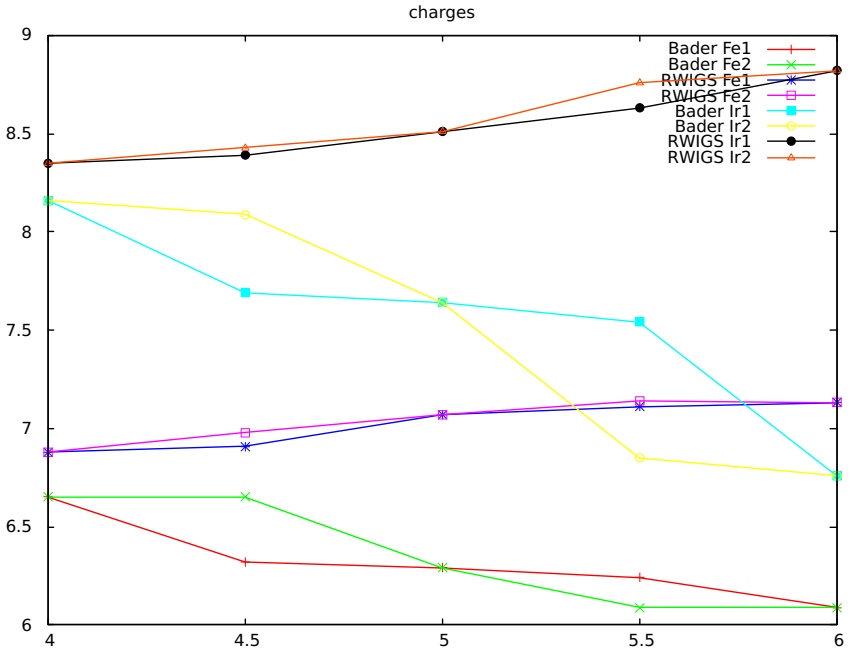

Figure 11: RWIGS and Bader charges

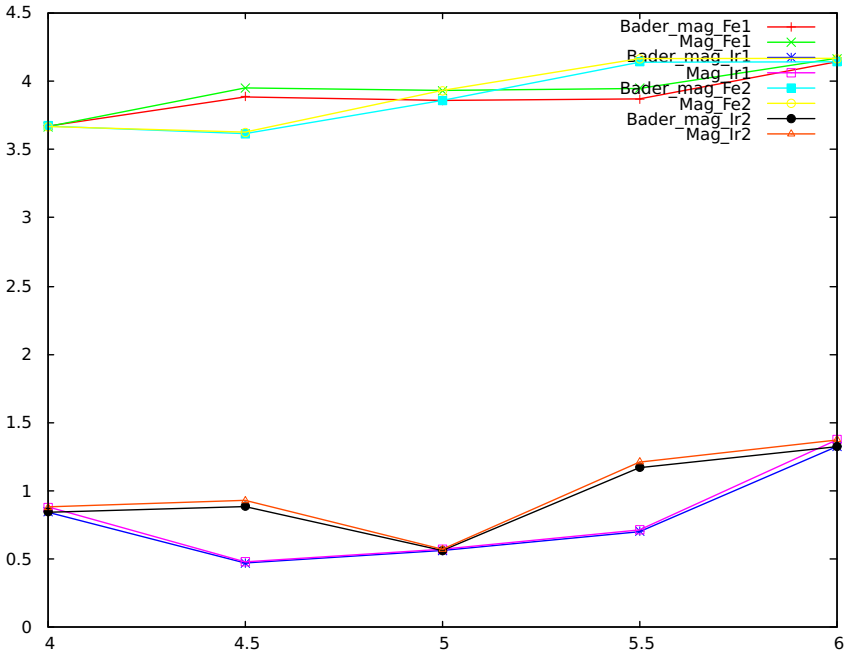

Figure 12: Magnetization

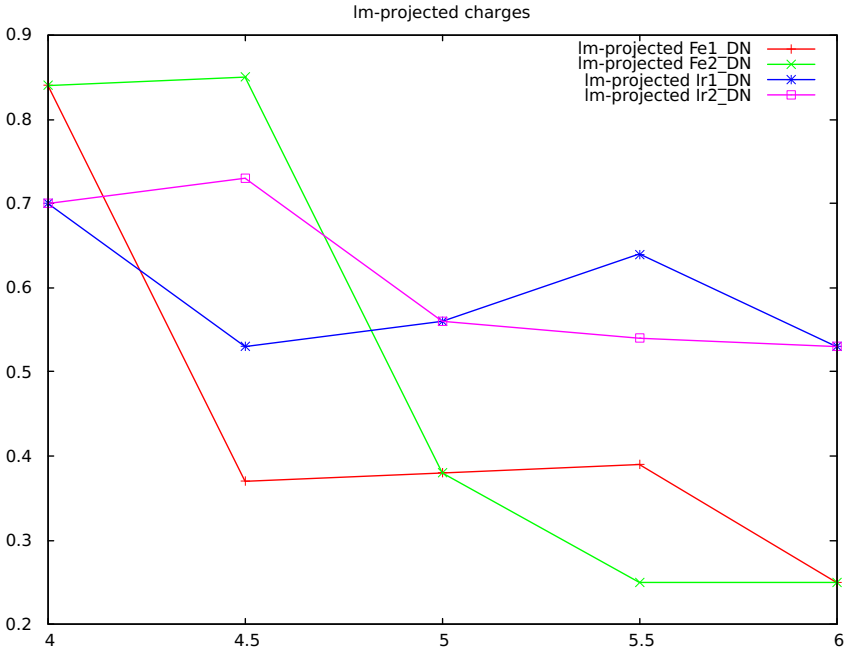

Figure 13: lm-decomposed charges

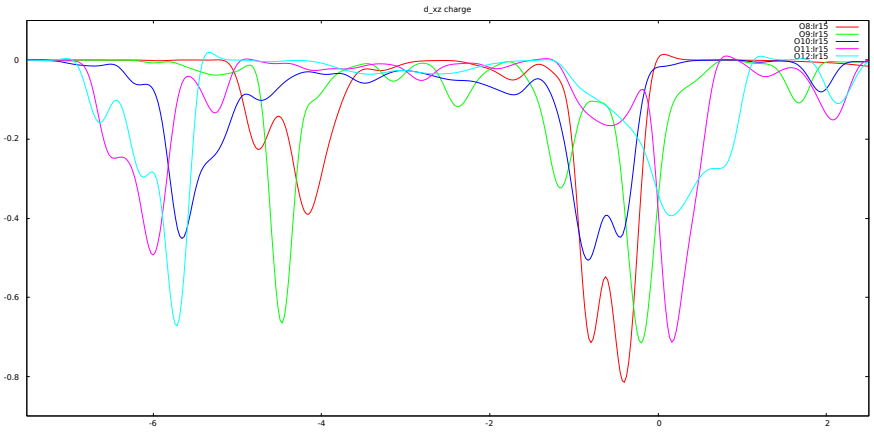

Figure 14: Bonding-antibonding gap of d_{xz} orbitals

radius and the extra electrons are distributed in interatomic areas.

References

[1] IV Solovyev, PH Dederichs, and VI Anisimov. Corrected atomic limit in the local-density approximation and the electronic structure of d impurities in rb. *Physical Review B*, 50(23):16861, 1994.

[2] Cédric Tassel, Takashi Watanabe, Yoshihiro Tsujimoto, Naoaki Hayashi, Atsushi Kitada, Yuji Sumida, Takafumi Yamamoto, Hiroshi Kageyama, Mikio Takano, and Kazuyoshi Yoshimura. Stability of the infinite layer structure with iron square planar coordination. *Journal of the American Chemical Society*, 130(12):3764–3765, 2008.